An-Najah University Journal for Research – A
Natural Sciences

Alignment Tolerance Specifications for Holographic OAM Generation: Quantifying Forked-Grating Misalignment Effects

Ayman Sweiti[1], Othman H. Y. Zalloum[*2]

(Type: Full Article). Received 04 February 2026, Accepted 11 March 2026, Published xxxx, DOI: xxxx

Accepted Manuscript, In Press

Abstract:
We establish the first quantitative alignment tolerance specifications for holographic generation of orbital angular momentum (OAM) beams, addressing a critical gap between optical design and mechanical implementation. While previous research focused on compensating intrinsic spatial light modulator imperfections, we provide a rigorous quantification of extrinsic transverse misalignment effects. Computational modeling of 1%–10% misalignments, combined with Hilbert–Schmidt fidelity analysis, reveals three operational regimes: **High-Fidelity** ($\leq$3%), **Critical** (4–5%), and **Severe Degradation** ($>$5%). The 3% threshold (approximately 475 μm for typical gratings) emerges as a critical design parameter for mounting systems and alignment stages. These quantitative guidelines are essential for transitioning OAM technologies from laboratory demonstrations to robust, field-deployable systems in optical communications and beam shaping.

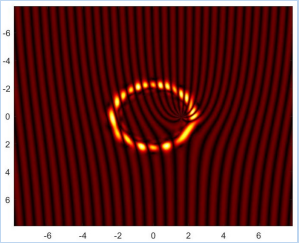

Keywords: Orbital angular momentum, Computer-generated holography, Alignment tolerance, Field fidelity, Hilbert-Schmidt inner product, Diffractive optics.

Research Highlights

- Quantitative framework for OAM beam alignment tolerance assessment
- Hilbert-Schmidt fidelity metric reveals three distinct operational regimes
- Critical threshold identified at 3% misalignment for precision applications
- Essential guidance for robust OAM system design and calibration

1 Introduction

Light's orbital angular momentum (OAM), described within the paraxial approximation, possesses both spin and orbital components along the propagation direction, as established by foundational studies [1, 2]. Its unique properties have enabled diverse applications, especially in optical communications [3, 4], including high-dimensional multiplexing and advanced beam shaping.

A critical challenge in practical OAM systems is precise alignment during high-purity OAM mode generation via computer-generated holography (CGH). Specifically, the incident Gaussian beam must be accurately centered on the singularity (the "fork" center) of the diffraction grating. Even minute transverse misalignments induce complex wavefront distortions that degrade mode purity, compromise beam quality, and reduce system performance across various applications.

Significant research efforts have focused on optimizing holographic OAM generation by correcting *intrinsic* device imperfections, such as phase modulation non-linearity and pixelated spatial light modulators (SLMs), which are known to reduce mode purity [5, 6]. Furthermore, artifacts like the splitting of desired modes into conjugate orders

[1]Department of Applied Mathematics and Physics,
College of Applied Sciences, Palestine Polytechnic University, Hebron, Palestine
E-mail: sweitia@ppu.edu
[2]Department of Applied Mathematics and Physics,
College of Applied Sciences, Palestine Polytechnic University, Hebron, Palestine
*Corresponding author e-mail: ozalloum@ppu.edu
ORCID: 0000-0001-7282-1332

have been mitigated through advanced grating design [7]. In contrast, while frequently acknowledged as experimentally relevant, *extrinsic* alignment errors—notably transverse beam misalignment—have been largely addressed only qualitatively.

Recent analytical frameworks [8, 9] have begun to rigorously quantify how lateral displacement and angular tilt affect the detected OAM spectrum, highlighting critical parameters that influence alignment sensitivity. However, a systematic quantification of alignment tolerance—defined as the maximum misalignment that maintains sufficient field fidelity—remains conspicuously absent from the literature. This gap between qualitative awareness and quantitative specification prevents the establishment of clear design rules, calibration protocols, and mechanical tolerance specifications for robust, field-deployable systems.

To address this critical gap, we introduce a comprehensive framework for quantifying alignment tolerance in holographic OAM generation. Our approach employs computational modeling with the Hilbert–Schmidt inner product as a fidelity metric, which provides a rigorous measure of field similarity by capturing both amplitude and phase distortions. Unlike intensity-based measures, this approach directly quantifies how misalignment degrades the complex field structure, offering insights that are essential for precision applications.

This study directly addresses this need by providing a systematic quantification of the primary *extrinsic* error source: transverse beam-to-grating misalignment. To our knowledge, this work yields the first explicit, fidelity-based tolerance thresholds for holographic OAM generation (e.g., $<$3% misalignment for $>$90% fidelity), establishing three distinct operational regimes with clear engineering implications. These quantitative guidelines provide actionable specifications for mechanical design, alignment procedures, and system calibration, thereby facilitating the transition of OAM applications from laboratory demonstrations to robust, real-world deployment.

2 Holographic Generation of Orbital Angular Momentum Beams

Laguerre-Gaussian (LG) modes form a complete orthogonal basis set for paraxial light beams in cylindrical coordinates. They are characterized by two indices: the azimuthal index ℓ (often denoted l), which determines the orbital angular momentum (OAM) content, and the radial index p, which governs the number of concentric rings in the intensity profile. A beam with $\ell \neq 0$ carries a helical phase front described by $\exp(i\ell\phi)$, where ϕ is the azimuthal angle; this helical phase gives rise to an optical vortex—a phase singularity—along the beam axis [3, 10]. The full complex amplitude of an LG mode is given by the product of a Gaussian envelope, a Laguerre polynomial describing the radial structure, and the helical phase term. Explicitly, for a Laguerre-Gaussian mode the amplitude [10, 11, 12, 3] is given by:

$$\begin{aligned} LG_{p,l} = &\sqrt{\frac{2p!}{\pi(p+|l|)!}}\frac{1}{w(z)}\left[\frac{r\sqrt{2}}{w(z)}\right]^{|l|} \\ &\times e^{-\frac{r^2}{w^2(z)}} L_p^{|l|}\left(\frac{2r^2}{w^2(z)}\right) e^{\frac{ik_0 r^2 z}{2(z^2+z_R^2)}} \\ &\times e^{-i(2p+|l|+1)\tan^{-1}\left(\frac{z}{z_R}\right)} \times e^{-il\phi} \end{aligned} \tag{1}$$

where the $1/e$ radius of the Gaussian beam is $w(z) = w(0)\left[(z^2+z_R^2)/z_R^2\right]^{1/2}$, with $w(0)$ being the beam waist, z_R the Rayleigh range, and $(2p+|l|+1)\tan^{-1}\left(\frac{z}{z_R}\right)$ representing the Gouy phase. The term $L_p^{|l|}$ denotes the generalized Laguerre polynomial.

Equation (1) can be expressed in compact form as:

$$\langle \vec{r}|k,l,p\rangle = \psi(r,z)_{klp}e^{-il\phi} \tag{2}$$

To examine the features of far-field diffraction patterns of OAM wavefronts using standard diffraction techniques, consider the schematic diagram in Figure 1a. The diffracting aperture lies in the (ξ, η) plane, illuminated in the positive z-direction. We calculate the wave field across the parallel (x, y) plane at normal distance z. The Fraunhofer far-field diffraction amplitude is given by

$$U(x,y) = \frac{e^{ikz}}{i\lambda z}e^{i\frac{k}{2z}(x^2+y^2)}\iint\limits_{\text{aperture}} U(\xi,\eta)e^{-i\frac{2\pi}{\lambda z}(x\xi+y\eta)}\,d\xi\,d\eta \tag{3}$$

The integral equation in (3) represents the Fourier transform of the hologram-modulated electric field multiplied by a scaling factor. The diffracting aperture is a thin amplitude computer-generated hologram containing the interference pattern between an object wave and a reference wave (Figure 1b). The reference wave is a plane wave $e^{i\vec{k}\cdot\vec{r}}$, while the primary wave corresponds to the paraxial region of a Laguerre-Gaussian beam carrying quantized orbital angular momentum (OAM) [13, 14, 15, 16, 3]. The hologram transmittance function is:

$$T(\eta,\xi) = \left|e^{i\vec{k}\cdot\vec{r}} + e^{-im\phi}\right|^2 \tag{4}$$

From Figure 1b, $\vec{k}\cdot\vec{r} = k\eta\sin\alpha$, yielding:

$$T(\eta,\xi) = e^{-i(m\phi+k\eta\sin\alpha)} + e^{i(m\phi+k\eta\sin\alpha)} + 2 \tag{5}$$

The transmitted electric field after grating illumination is:

$$U(\eta,\xi) = T(\eta,\xi)\,LG_{p,l}(\eta,\xi) \tag{6}$$

Using the compact LG-mode form (Eq. 2), the far-field diffraction becomes:

$$\begin{aligned} U(x,y) = &\frac{e^{ikz}}{i\lambda z}e^{i\frac{k}{2z}(x^2+y^2)}\times \\ &\iint\limits_{\text{aperture}}\left(e^{-i((m+l)\phi+k\eta\sin\alpha)} + e^{i((m-l)\phi+k\eta\sin\alpha)} + 2e^{-il\phi}\right) \\ &\times\left[\psi(r,z)_{klp}e^{-i\frac{2\pi}{\lambda z}(x\xi+y\eta)}\right]d\xi d\eta \end{aligned} \tag{7}$$

where $\phi = \phi(\eta,\xi)$. Equation (7) contains holographic information for the zeroth and first orders, with OAM values of $L = m\hbar$ and $L = (m\pm l)\hbar$ respectively.

3 Computational Modeling of Transverse Misalignment

To simulate transverse misalignment in the laser beam-diffraction grating system, we introduce relative shifts along $\hat{\xi}$ and $\hat{\eta}$ by amounts ξ_0 and η_0. Equation (4) then becomes:

$$T(\eta,\xi) = \left|e^{i\frac{2\pi}{\Lambda}\eta_t\sin\alpha} + e^{-im\phi_t}\right|^2 \tag{8}$$

where η_t and ϕ_t are transformed coordinates after displacement, and Λ is the grating period. The azimuthal angle transforms as follows:

$$\phi_t(\eta,\xi) = \operatorname{atan2}(\xi-\xi_0, \eta-\eta_0) \tag{9}$$

Applying the same translation to the plane wave component yields:

$$T_t(\eta,\xi) = \left|e^{i\frac{2\pi}{\Lambda}(\eta-\eta_0)\sin\alpha} + e^{-im\phi_t}\right|^2 \tag{10}$$

Using Equation (10), we computationally generated amplitude-modulated CGHs (Figure 2) from the coherent superposition of a plane wave and an LG mode with $\ell = 10$. The grating period is $\Lambda = 264$ μm with dimensions 15.8 $\times$ 15.8 mm. For demonstration purposes, the number of grating lines was reduced to 30 to ensure visibility.

Figure 2 shows the calculated amplitude diffraction gratings with the laser beam overlaid for perfect alignment (panel b) and for 10 % transverse misalignment in the x-direction (panel a) and y-direction (panel c).

The transmitted electric field is:

$$U(\eta,\xi) = T_t(\eta,\xi)LG_{l,p}(\eta,\xi) \tag{11}$$

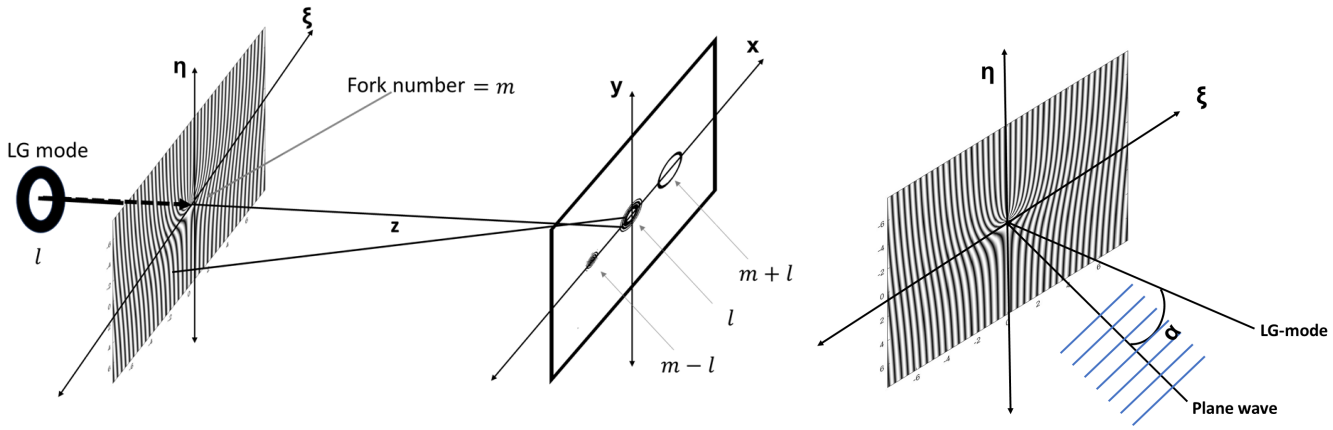

(a) Experimental setup schematic

(b) Computer-generated hologram

Figure 1: Diffraction geometry and grating structure

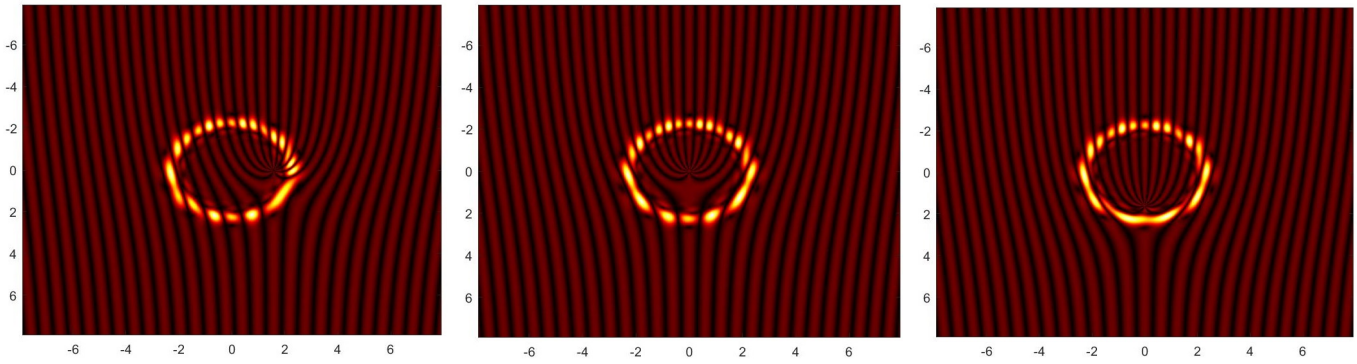

(a) 10% x-shift misalignment

(b) Zero shift (perfect alignment)

(c) 10% y-shift misalignment

Figure 2: Calculated amplitude diffraction gratings with overlaid laser beam showing transverse alignment shifts (scale in mm). Panels (a), (b), and (c) show the laser beam overlaid on the grating at 10% x-shift misalignment, perfect alignment (zero shift), and 10% y-shift misalignment, respectively.

where T_t is the transversely shifted grating function. Given the observation distance substantially exceeds the aperture size, we employed Fraunhofer approximation (Eq. 3) to compute diffraction amplitudes:

$$U(x,y) = \frac{e^{ikz}}{i\lambda z} e^{i\frac{k}{2z}(x^2+y^2)} \iint_{\text{aperture}} \left| e^{i\frac{2\pi}{\Lambda}(\eta-\eta_0)\sin\alpha} + e^{-im\phi_t} \right|^2 \times \sqrt{\frac{2p!}{\pi(p+|l|)!}} \frac{1}{w(z)} \left[\frac{r\sqrt{2}}{w(z)}\right]^{|l|} e^{-\left[\frac{r^2}{w^2(z)}\right]} \times L_p^{|l|}\left(\frac{2r^2}{w^2(z)}\right) \times e^{\left[\frac{ik_0 r^2 z}{2(z^2+z_R^2)}\right]} e^{-i(2p+|l|+1)\tan^{-1}\left(\frac{z}{z_R}\right)} e^{-il\phi} \times e^{-i\frac{2\pi}{\lambda z}(x\xi+y\eta)}\, d\xi\, d\eta \tag{12}$$

3.1 Numerical Implementation

All numerical simulations and computational modeling in this study were performed using MATLAB (MathWorks, Natick, MA, USA) [17]. MATLAB's robust numerical integration and matrix manipulation capabilities were utilized to implement the holographic generation model and to compute far-field diffraction patterns based on the Fraunhofer approximation (Eq. 12).

The Laguerre-Gaussian beam modes, hologram transmittance functions, and shifted coordinate transformations were coded using MATLAB's built-in mathematical functions. Complex field matrices representing the first-order diffracted OAM beams were computed and stored as 701×701 element arrays. The Hilbert-Schmidt inner product metric (Eq. 13) for fidelity calculations was implemented via standard matrix operations in MATLAB.

Simulation parameters (wavelength, beam waist, grating dimensions, misalignment increments) were all specified explicitly within the MATLAB code, ensuring repeatability and transparency of the numerical experiments. Visualization of intensity and phase distributions was performed using MATLAB's graphical plotting toolkits.

This computational approach provided a flexible and precise platform for systematic investigation of misalignment effects on holographically generated OAM beams.

4 Results and Analysis

4.1 First-Order Diffraction Amplitudes and Phase Structure

The analysis focuses on quantifying field distortion due to transverse misalignment by examining first-order diffraction amplitudes corresponding to an $\ell = 20$ Laguerre-Gaussian (LG) mode. Complex field amplitude arrays were computationally extracted from the total diffracted field and organized as 701×701 element matrices. To ensure accurate fidelity comparisons, these matrices were spatially registered to compensate for transverse displacements introduced by misalignment, maintaining consistent coordinate systems across all conditions. The phase angle of each field element was calculated as $\theta_{ij} = \operatorname{atan2}(U_{ij}^{\text{im}}, U_{ij}^{\text{re}})$, yielding values in $(-\pi, \pi)$. Figures 3c and 3d display the extracted first-order field and its phase structure, which serves as the reference for fidelity calculations.

Figure 4 systematically presents intensity distributions ($I_{ij} = U_{ij}^* U_{ij}$) and corresponding phase structures across a range of transverse shifts. Visual analysis reveals initial phase structure modifications becoming discernible at 2% shift, with more significant anomalies emerging at 4% shift, including the development of an extra line in the fork structure. This topological defect indicates substantial deviation from the pure $\ell = 20$ LG-mode topology, representing intrusion of parasitic OAM modes and direct evidence of mode purity degradation. The progressive deterioration visible in these phase maps provides compelling qualitative evidence of the system's sensitivity to misalignment, establishing the foundation for quantitative fidelity analysis.

4.2 Field Similarity Quantification and Operational Regimes

The projection fidelity of misaligned fields onto the reference field was calculated using the Hilbert-Schmidt inner product, defined as:

$$\mathcal{F} = \sqrt{\frac{\langle \mathbf{U}_{\text{ref}}, \mathbf{U}\rangle_{\text{HS}} \langle \mathbf{U}, \mathbf{U}_{\text{ref}}\rangle_{\text{HS}}}{\langle \mathbf{U}_{\text{ref}}, \mathbf{U}_{\text{ref}}\rangle_{\text{HS}} \langle \mathbf{U}, \mathbf{U}\rangle_{\text{HS}}}} \times 100\%, \tag{13}$$

where $\mathbf{U}_{\text{ref}}$ denotes the reference complex field, $\mathbf{U}$ represents the misaligned field, and $\langle \mathbf{U}_1, \mathbf{U}_2\rangle_{\text{HS}} = \text{Tr}(\mathbf{U}_1^\dagger \mathbf{U}_2)$ is the Hilbert-Schmidt inner product. This metric provides a normalized measure of field similarity that captures both amplitude and phase distortions.

Application of Equation (13) to 701×701 element matrices revealed three distinct operational regimes with clear quantitative boundaries (Figure 5 and Table 1):

High-Fidelity Regime ($\leq$3% shift): Field fidelity remains above 94.6%, with minimal degradation even at 3% misalignment. This regime preserves the essential topological characteristics of the $\ell = 20$ mode, making it suitable for applications demanding high mode purity.

Critical Degradation Regime (4–5% shift): Fidelity drops to 77.7–89.1%, representing a transitional zone where field distortion becomes significant. The 5% threshold marks a particularly critical point where fidelity falls below 80% along the x-direction, indicating substantial mode mixing.

Severe Degradation Regime ($>$5% shift): Fidelity collapses below 68.8%, with values as low as 19.6% at 9% misalignment. This regime exhibits severe field distortion where the generated beam bears little resemblance to the target $\ell = 20$ mode.

For misalignments exceeding 4%, we observe systematic differences between X- and Y-direction fidelity values. As shown in Table 1, Y-shifts consistently yield higher fidelity than X-shifts across the 5–9% misalignment range, with the disparity reaching approximately 15–16 percentage points at 7–9% misalignment. This asymmetry originates from the vertical orientation of the fork dislocation in our hologram design. The creation of helical wavefronts using CGH depends on an on-axis fork dislocation where one or more grating lines terminate abruptly at the center. For Y-shifts, the center of the forked structure is illuminated, covering all terminating lines symmetrically, whereas X-shifts displace the beam away from the center, causing asymmetric illumination and greater phase distortion. At 10% misalignment, we observe a reversal where X-fidelity (32.1%) slightly exceeds Y-fidelity (26.8%). This non-monotonic behavior likely arises from the beam sampling multiple grating periods at extreme shifts, introducing complex interference and phase-wrapping effects that differentially affect the two orthogonal directions.

The x- and y-directional responses show near symmetry up to 5% misalignment, with divergence becoming progressively more pronounced at larger shifts. For practical engineering purposes, the directional differences are negligible within the High-Fidelity regime ($\leq$3%) and become relevant only in the Severe Degradation regime where fidelity is already below acceptable thresholds for most applications. This near-isotropic behavior within the critical 3% tolerance window further supports the use of a single percentage-based specification for mechanical design and alignment procedures.

5 Discussion

The quantitative alignment tolerance thresholds established in this study provide actionable specifications for the design and implemen-

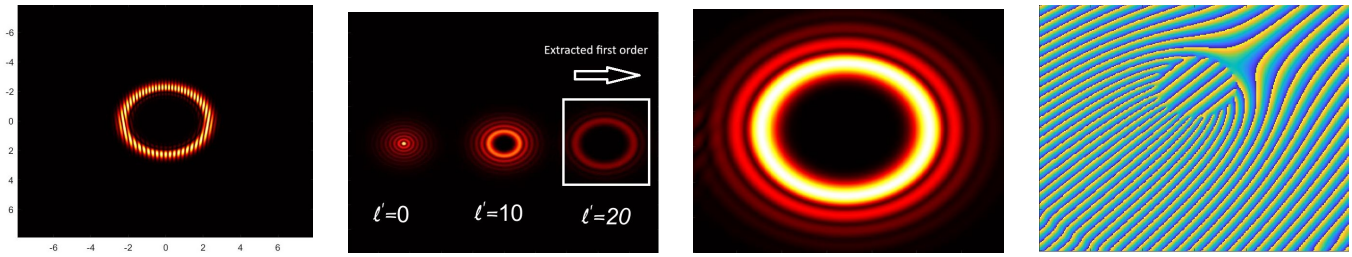

(a) Aligned illumination (b) Far-field pattern (c) First-order diffraction (d) Phase structure

Figure 3: Reference field (zero shift configuration): (a) Grating illumination pattern, (b) Far-field diffraction profile, (c) Extracted first-order component, (d) Corresponding phase structure

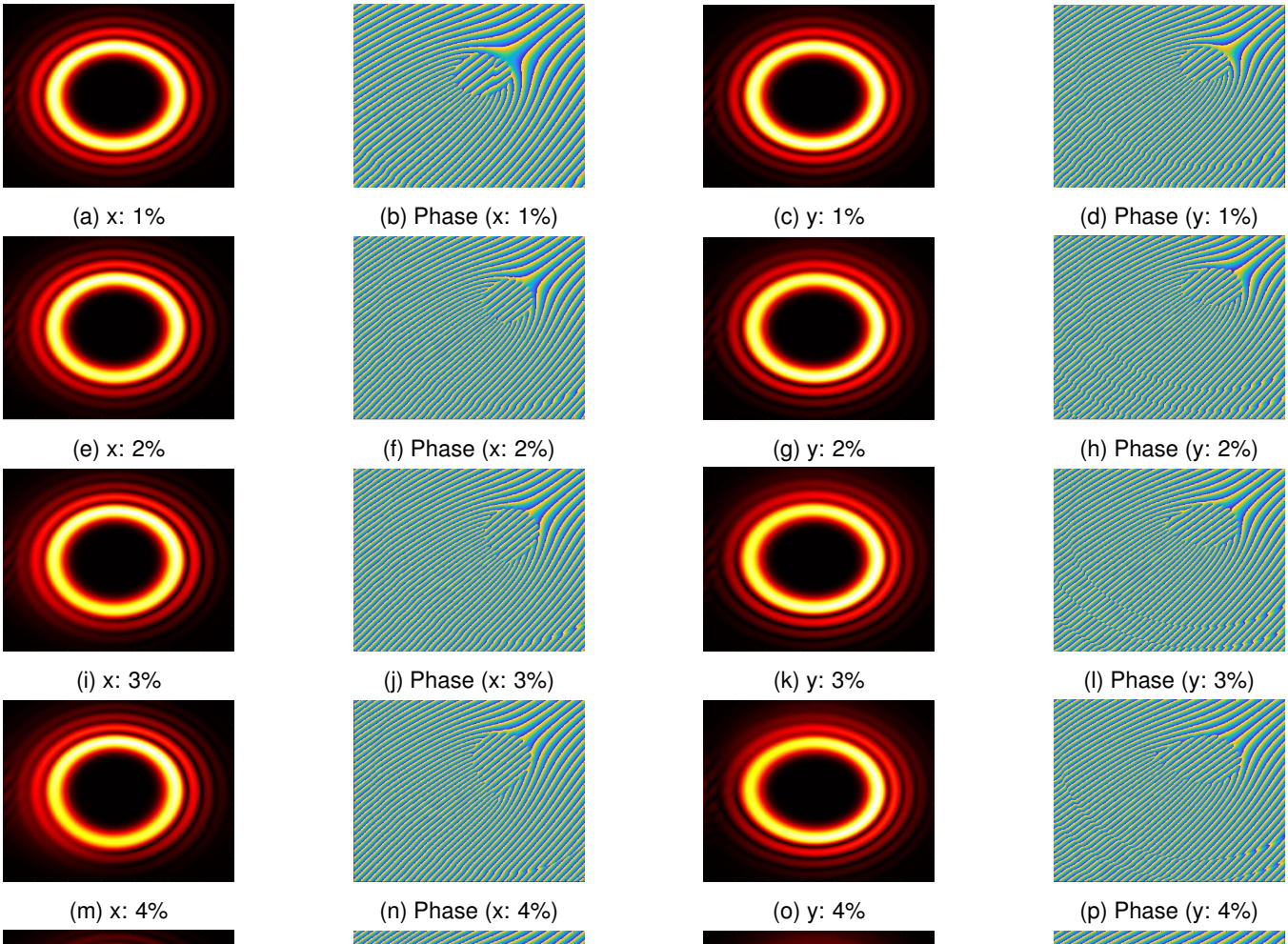

(a) x: 1% (b) Phase (x: 1%) (c) y: 1% (d) Phase (y: 1%)

(e) x: 2% (f) Phase (x: 2%) (g) y: 2% (h) Phase (y: 2%)

(i) x: 3% (j) Phase (x: 3%) (k) y: 3% (l) Phase (y: 3%)

(m) x: 4% (n) Phase (x: 4%) (o) y: 4% (p) Phase (y: 4%)

(q) x: 6% (r) Phase (x: 6%) (s) y: 6% (t) Phase (y: 6%)

Figure 4: Extracted first-order diffraction patterns and corresponding phase structures for transverse misalignments along x and y directions, demonstrating progressive degradation with increasing shift magnitude

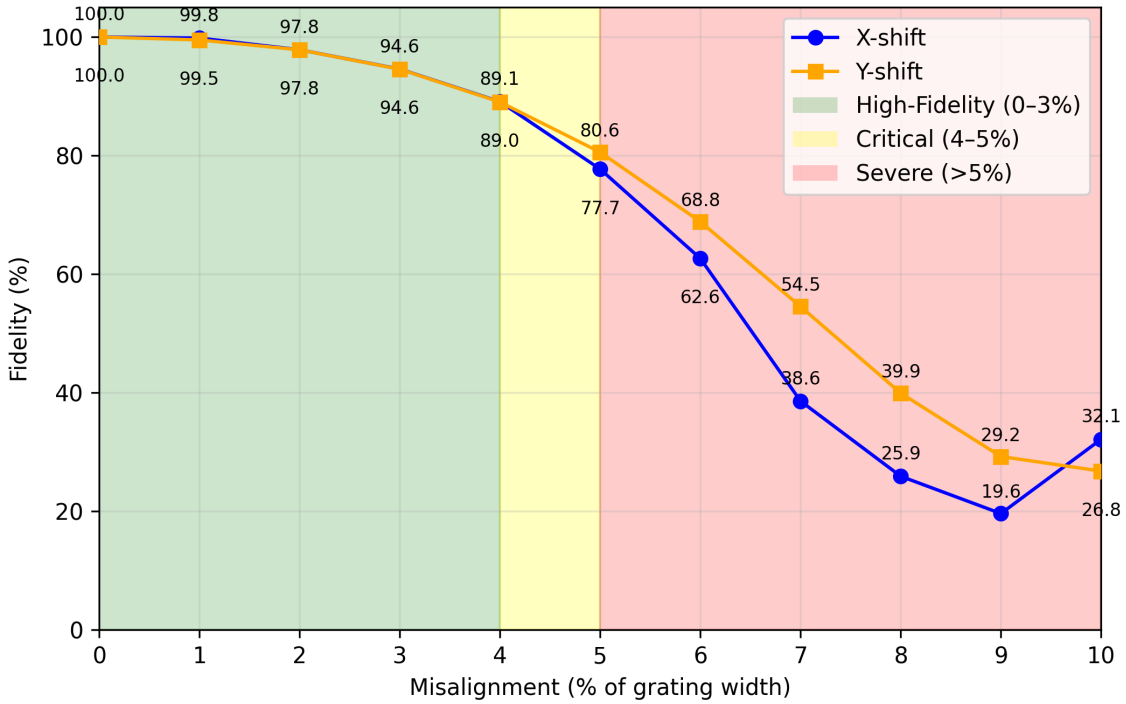

Figure 5: Projection fidelity of misaligned first-order fields onto the reference aligned field versus misalignment percentage. Blue circles and solid line represent X-direction shifts; orange squares and solid line represent Y-direction shifts. Vertical shaded bands indicate operational regimes: High-Fidelity (0–3%), Critical (4–5%), and Severe Degradation (>5%). The plot demonstrates near-isotropic behavior up to 5% misalignment, with directional divergence emerging at larger shifts.

Table 1: Quantitative fidelity assessment at key misalignment thresholds (3 s.f.)

Misalignment (% width)	**X-Fidelity (%)**	**Y-Fidelity (%)**
0	100	100
1	99.8	99.5
2	97.8	97.8
3	94.6	94.6
4	89.1	89.0
5	77.7	80.6
6	62.6	68.8
7	38.6	54.5
8	25.9	39.9
9	19.6	29.2
10	32.1	26.8

tation of holographic OAM systems. By linking percentage misalignment to field fidelity, we bridge the gap between qualitative alignment awareness and quantitative engineering requirements.
These findings directly address the gap identified in the introduction between qualitative awareness of alignment importance and quantitative specifications for mechanical design. The transition from "alignment matters" to "alignment must be within 475 μm" represents a critical step toward engineering robust OAM systems.

5.1 Validation and Practical Implications

Independent validation through LG mode reconstruction from phase patterns confirms the fidelity thresholds. Converting phase patterns to thin amplitude gratings and illuminating with plane waves reconstructed the modes, with diffraction pattern intensities serving as quality indicators. Visual comparison of vortex shapes (Figure 6) shows preserved structural integrity for misalignments up to 3%, with observable degradation at 4% and severe distortion at 5%, corroborating the quantitative fidelity analysis.
The alignment tolerance thresholds translate directly into engineering specifications. For our 15.8 mm grating, the critical 3% tolerance corresponds to approximately 475 μm. This concrete specification informs mechanical design parameters for mounting fixtures, alignment stages, and environmental stability requirements. Systems requiring high mode purity should maintain alignment within this 3% window, while applications with moderate requirements might accept the 4–5% critical regime with appropriate performance trade-offs.

5.2 Comparative Context and System Design Implications

The sensitivity revealed in this study (90% fidelity drop at 5% misalignment) exceeds that of conventional Gaussian beam systems, which typically tolerate 10–15% misalignment before significant coupling loss. This heightened sensitivity stems from the topological nature of OAM modes and their phase singularities, which are particularly vulnerable to misalignment-induced distortions.
Higher-order OAM modes exhibit even greater sensitivity due to their larger spatial extent and more complex phase structures [8, 4]. This creates a scalability challenge for high-dimensional systems, where maintaining alignment across multiple modes becomes increasingly demanding. Our findings suggest that system designs should incorporate:

1. Mechanical stability specifications based on the 3% tolerance threshold.
2. Active alignment systems with sub-3% precision for demanding applications.
3. Integrated alignment markers in grating designs to facilitate calibration.
4. Regular alignment verification protocols during system operation.

The directional asymmetry observed for misalignments exceeding 4% (Section 4.2) has practical implications for system design. The vertical orientation of the fork dislocation makes the hologram more sensitive to displacements perpendicular to the fork line (x-direction) than parallel to it (y-direction). This suggests that if a system has tighter mechanical tolerances or better active stabilization in one axis, the grating should be oriented so that the more sensitive direction aligns with the better-controlled axis. Conversely, applications requiring isotropic alignment tolerance may benefit from alternative hologram designs with circularly symmetric phase structures. However, for most practical purposes, the 3% tolerance threshold remains the primary design specification, as directional differences are negligible within this high-fidelity window.
While adaptive optics and dynamic beam tracking offer potential mitigation [4], these approaches increase system complexity and cost. The quantitative thresholds provided here enable cost-benefit analysis of such compensation strategies versus improving passive mechanical stability.

5.3 Limitations and Future Work

This study focuses specifically on transverse misalignment for a single $\ell = 20$ mode. Looking forward, several avenues for future work emerge:

1. **Experimental validation** of these computational thresholds through controlled misalignment measurements.
2. **Extension to different OAM orders** to establish scaling relationships between mode complexity and alignment sensitivity.
3. **Investigation of combined misalignment effects** including angular tilt, defocus, and rotational errors.
4. **Application of this framework to superposition states and mode division multiplexing scenarios**.

While this study concentrates on a specific $\ell = 20$ mode and transverse misalignment, the methodological framework established here provides a foundation for broader tolerance analysis in holographic OAM systems. By providing quantitative alignment tolerance specifications and a methodological framework for their assessment, this work contributes to the maturation of OAM technologies from laboratory demonstrations to robust, field-deployable systems. These findings offer essential guidance for optical engineers designing next-generation communication links, beam shaping systems, and other applications where precise control of complex optical fields is paramount.

6 Conclusion

This study has successfully established the first quantitative tolerance thresholds for transverse misalignment in holographic OAM beam generation. Using a Hilbert–Schmidt fidelity metric that captures both amplitude and phase distortions, we identified three distinct operational regimes with clear engineering implications: **High-Fidelity** ($\leq$3% misalignment), **Critical Degradation** (4–5%), and **Severe Degradation** ($>$5%). These regimes provide more than just qualitative guidelines—they offer concrete specifications that bridge the gap between optical design and mechanical implementation.
The 3% tolerance threshold, corresponding to approximately 475 μm for a 15.8 mm grating, establishes a critical design parameter for mounting systems, alignment stages, and environmental stability requirements. Our findings reveal that holographic OAM generation exhibits significantly higher sensitivity to misalignment compared to conventional Gaussian beam systems, underscoring the need for specialized alignment procedures in OAM-based applications.
The Hilbert–Schmidt fidelity metric provides a generalizable framework that can be adapted to assess other alignment-sensitive parameters in diffractive optical systems. The three-regime model (high-fidelity, critical, severe) offers a structured approach to categorize system performance and define application-specific acceptance criteria.
By establishing quantitative alignment tolerance specifications and providing a methodological framework for tolerance analysis, this work contributes to the maturation of OAM-based technologies from laboratory demonstrations to robust, field-deployable systems. The fidelity thresholds and operational regimes identified here serve as essential guidelines for optical engineers designing next-generation communication and beam shaping systems.

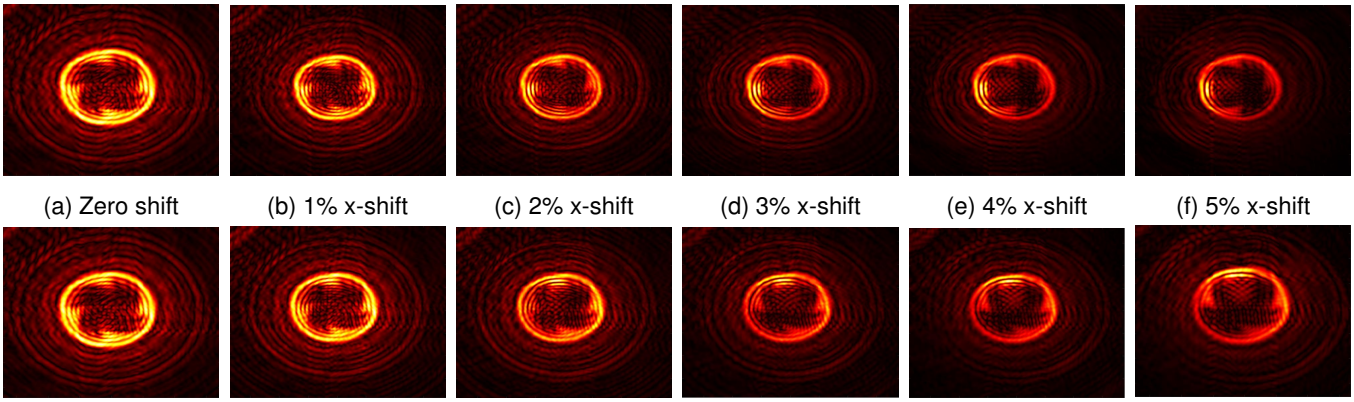

(a) Zero shift (b) 1% x-shift (c) 2% x-shift (d) 3% x-shift (e) 4% x-shift (f) 5% x-shift

(g) Zero shift (h) 1% y-shift (i) 2% y-shift (j) 3% y-shift (k) 4% y-shift (l) 5% y-shift

Figure 6: Reconstructed first-order LG modes from phase structures showing progressive degradation with increasing misalignment. Top row: x-direction shifts (0–5%); bottom row: y-direction shifts (0–5%). The zero-shift case is repeated for visual reference.

Ethics approval and consent to participate

Not applicable

Consent for publication

Not applicable

Availability of data and materials

The raw data required to reproduce these findings are available in the body and illustrations of this manuscript.

Author Contributions

Ayman Sweiti: Conceptualization, Methodology, Software, Validation, Formal analysis, Investigation, Writing – original draft, Visualization. **Othman H. Y. Zalloum:** Conceptualization, Resources, Writing – review & editing, Project administration, Corresponding author.
In addition, O.H.Y.Z. made substantial contributions to the writing, editing, and revision of the whole manuscript.
Both authors have read and approved the final version of the manuscript.

Funding

This research received no external funding.

Conflicts of interest

The authors declare that there is no conflict of interest regarding the publication of this article.

Acknowledgements

The authors acknowledge the support of Palestine Polytechnic University.

References

[1] Allen L, Beijersbergen MW, Spreeuw RJC, Woerdman JP. Orbital angular momentum of light and the transformation of Laguerre-Gaussian laser modes. *Phys Rev A*. 1992;45(11):8185–8189.

[2] Padgett MJ. Orbital angular momentum 25 years on. *Opt Express*. 2016;25(10):11265–11274.

[3] Yao AM, Padgett MJ. Orbital angular momentum: origins, behavior and applications. *Adv Opt Photon*. 2011;3(2):161–204.

[4] Willner AE, Huang H, Yan Y, Ren Y, Ahmed N, Xie G, Bao C, Li L, Cao Y, Willner AZ, Ashrafi S, Tur M, Ashrafi S, Molisch AF. Optical communications using orbital angular momentum beams. *Adv Opt Photon*. 2021;13(3):772–852.

[5] Márquez A, Iemmi C, Moreno I, Davis JA, Campos J, Yzuel MJ. Quantitative prediction of the modulation behavior of twisted nematic liquid crystal displays based on a simple physical model. *Opt Eng*. 2001;40(11):2558–2564.

[6] Igasaki Y, Li F, Yoshida N, Toyoda H, Inoue T, Mukohzaka N, Kobayashi Y, Hara T. High efficiency electrically-addressable phase-only spatial light modulator. *Opt Rev*. 1999;6(4):339–344.

[7] Gruneisen MT, Dymale RC, Raymond TD. Holographic generation of complex optical fields for diffraction-limited focusing. *Opt Express*. 2008;16(26):21338–21350.

[8] Jha AK, Agarwal GS. Effect of misalignment on the orbital angular momentum spectrum of light beams. *J Opt Soc Am A*. 2025;42(1):A1–A8.

[9] Jha AK, Agarwal GS. Sensitivity of orbital angular momentum modes to lateral displacement and tilt. *Phys Rev A*. 2025;101(2):023843.

[10] Allen L, Padgett MJ, Babiker M. The orbital angular momentum of light. *Prog Opt*. 1999;39:291–372.

[11] Kolobov MI, editor. *Quantum Imaging*. New York: Springer; 2007.

[12] Siegman AE. *Lasers*. Mill Valley, CA: University Science Books; 1986.

[13] Gibson G, Courtial J, Padgett MJ, Vasnetsov M, Pas'ko V, Barnett SM, Franke-Arnold S. Free-space information transfer using light beams carrying orbital angular momentum. *Opt Express*. 2004;12(22):5448–5456.

[14] Barnett SM, Babiker M, Padgett MJ. Optical orbital angular momentum. *Philos Trans R Soc A*. 2016;375(2087):20150444.

[15] Sacks ZS, Rozas D, Swartzlander GA. Holographic formation of optical-vortex filaments. *J Opt Soc Am B*. 1998;15(8):2226–2234.

[16] Bekshaev AY, Soskin MS, Vasnetsov MV. *Paraxial Light Beams with Angular Momentum*. Nova Science Publishers; 2011.

[17] MATLAB. Version R2021a. Natick, Massachusetts: The MathWorks Inc.; 2021.